Electricity-driven selectivity in the photocatalytic oxidation of methane to carbon monoxide with liquid gallium-semiconductor composite

My Nghe Tran, Alina Skorynina, Ahmed Addad, Ali Fadel, Karima Ben Tayeb, Lydia Karmazin, Louis Thomas, Massimo Corda, Yevkeni Wisse, Evgeny Vovk, et al.

Electricity-driven selectivity in the photocatalytic oxidation of methane to carbon monoxide with liquid gallium-semiconductor composite

M. Nghe Tran[1,2], A. Skorynina[3], A. Addad[4], A. Fadel[5], K.B. Tayeb[6], L. Karmazin[5], L. Thomas[2], M. Corda[1], Y. Wisse[1], O. Vovk[1], A.Y. Khodakov[1], B. Grandidier[2*], V. Ordomsky[1*]

[1] *Univ. Lille, CNRS, Centrale Lille, ENSCL, Univ. Artois, UMR 8181 – UCCS – Unité de Catalyse et Chimie du Solide, F-59000 Lille, France*

[2] *Univ. Lille, CNRS, Centrale Lille, Univ. Polytechnique Hauts-de-France, Junia-ISEN, UMR 8520 - IEMN, F-59000 Lille, France*

[3]*CELLS-ALBA Synchrotron Radiation Facility, Carrer de la Llum 2-26, 08290 Cerdanyola del Vallès, Spain.*

[4]*CNRS, INRAE, Centrale Lille, UMR 8207 - UMET - Unité Matériaux et Transformations, Université de Lille, Lille F-59000, France.*

[5]*Univ. Lille, CNRS, INRAE, Centrale Lille, Université d'Artois, FR 2638–IMEC-Institut Michel-Eugene Chevreul, 59000 Lille, France.*

[6]*University of Lille, CNRS, UMR 8516 – LASIRE – Laboratoire de Spectroscopie pour les Interactions, la Réactivité et l'Environnement, F-59000 Lille, France*

**Corresponding authors*

Abstract

Metal co-catalysts in oxide semiconductors are essential to enhance photocatalytic reaction, but the selectivity is often low due to the conversion of the target molecules as more reactive in comparison with the reagents. Here, we explore the influence of electricity on the activity and selectivity of liquid gallium as a co-catalyst loaded in TiO_2 and ZSM-5 supports the photocatalytic oxidation of methane. We first show that the polarization of the photocatalytic chips allows a more efficient wetting of liquid gallium into the semiconductor matrices, which increases the availability of the photogenerated charge carriers for reactions and improves the overall activity of the composites. More importantly, the oxide skin surrounding the spread liquid is found to be charged, resulting in a significant reduction of the CO oxidation. An increase of the CO selectivity from 10 to 80 % upon polarization to 50 V, with a stable photocatalytic activity reaching 0.6 ± 0.01 mmol/g·h, makes the use of electricity quite appealing to tailor liquid metals in catalysis.

Keywords: Ga liquid metals, external electricity, photocatalytic methane conversion.

1. Introduction

Methane (CH_4) has been imposing a global warming threat of 30 times greater than carbon dioxide (CO_2) due to its abundance, powerful combustion, and wide usage in several sectors. At the moment the main industrial routes for conversion of methane are dry and steam reforming and partial oxidation of methane to produce syngas (CO and hydrogen). However, these routes require extremely high temperatures (>600 ºC) [1–4]. As photocatalysis offers an opportunity to perform the methane conversion at ambient temperature conditions by bypassing the thermodynamic limitations [5], partial photocatalytic oxidation of methane has been widely studied in literature (**Table S1, SI**) [6]. So far, the reaction has produced a significant amount of CO_2 due to the further oxidation of CO as a more reactive molecule than methane [7,8].

Photocatalysis relies on the absorption of photons. But the use of semiconductor absorbers is generally limited because of useless recombination between the photogenerated charge carriers, preventing them from activating the reactants. As a result, semiconductor photocatalysts are associated with metal co-catalysts (Pt, Pd, Au,…)[9,10]. These metal nanoparticles are known to strongly reduce the recombination process by scavenging one type of charge carriers [11,12], and, at the same time, provide additional reactive sites. Studies of the reaction efficiency as a function of the loading of solid metal co-catalysts have revealed that the highest activity occurs for small loadings only, about 1 wt% [13]. Higher loadings block the incident light to the semiconductor, reduce its surface-active sites and may even poison these sites once deposited in the host matrix. There is thus a quest to tailor metal co-catalysts

so that the efficiency and/or the selectivity of the reaction can be further improved. The use of metals such as gallium (Ga), becoming a liquid at near room temperature (29.8 ^{o}C) offers an opportunity to address this issue [14–16]. In its liquid form, it has been shown to act as a washing fluid, with a strong ability to remove precipitated byproducts, this self-regeneration property of the catalyst surface prolonging the catalyst lifetimes [17–19].

Here we investigate the influence of liquid Ga on the photocatalytic oxidation of methane to CO with two prototypical oxide semiconductors, TiO_2 and H-ZSM-5. At the melting point of Ga and upon the application of an external electric field across both composites, we find a reproducible enhancement of the total gas production. We show that the polarization of the catalytic chips results in a stronger wettability of the semiconductor supports. The interfacial area in the composite extends and favors the transfer of charge carrier for the activation of the reactants instead of their recombination. More importantly, a drastic change of selectivity is obtained when the chips are polarized: the selectivity to CO increasing from 10 to 80 %. Monitoring the oxidation of Ga with X-ray absorption spectroscopy evidences a regulation of the oxide skin around the spread liquid, when the chips are run with electricity. The skin is kept thin enough, so that the electrons transferred to Ga continuously tunnel across the skin, repelling the CO molecules and hence suppress their oxidation to CO_2 over the charged Ga surface. The opportunity to tailor the wetting and the interfacial charges of liquid metal with electricity is a very promising route to control selectivity in photocatalysis.

2. Material and methods

2.1. Materials and reagents

Gallium (Ga, 99.99% trace metals basis), titanium (IV) oxide powder (TiO_2, P25, 99.5%), and gallium (III) nitrate hydrate ($Ga(NO_3)_3.xH_2O$), were provided from Sigma-Aldrich. NH_4-ZSM-5 (CBV2314) with a SiO_2/Al_2O_3 ratio of 23 was purchased from Zeolyst. Nitrogen gas, methane and synthetic air were provided by Air Liquide company. All chemicals were used without further purification.

2.2. Fabrication of photocatalytic chips

First, H-ZSM-5 powder was prepared via the calcination of NH_4-ZSM-5 compound at 550 °C (ramp of 2 °C/min) for 6 hours under air medium, then the obtained powder was collected and stored for further steps [17]. The gallium (Ga) liquid metal-based photocatalysts were simply synthesized in a metallic reactor by mixing certain amounts of Ga metal with H-ZSM-5 and TiO_2, as a weight ratio of 1:1, then the powder mixtures were stirred and heated at 250 ^oC under N_2 medium (2 MPa) for 20 hours. After being cooled to room temperature, the obtained powders were ground and collected for photocatalytic tests (as illustrated in **Figure S1a**). For comparison, a Ga_2O_3/TiO_2 composite was prepared via incipient wetness impregnation of the $Ga(NO_3)_3$ aqueous solution and TiO_2 powder (Ga loading content of 5 wt%). Afterward, the sample was dried at 60 °C overnight and then calcined at 250 ^oC for 3 hours. In order to prepare the chips, gold electrodes were deposited on the glass substrates (2.5 cm × 2.5 cm) using a metal evaporation machine (the Plassys MEB E-beam 550S, as seen in **Figure S2, SI**), as described in a previous study [12]. Eventually, 20 mg of each catalyst powder was

dissolved in DI water (1 mL) and then transferred on the whole surface of the chips via drop-casting to study photocatalytic reactions (**Figure S1b, SI**).

2.3. Characterization and measurement

The morphology and chemical composition of the photocatalysts were investigated with a scanning electron microscope (SEM, JEOL) and with a scanning transmission electron microscope (S/TEM, TITAN Themis 300) mounted with an HAADF detector (electron energy of 300 keV). Energy-dispersive X-ray spectroscopy (EDS) was used to identify the chemical composition of the photocatalyst by acquiring element maps. The photoluminescence (PL) spectra were conducted with a 325 nm excitation (HR Labram, Horiba Scientific). The X-ray photoelectron spectroscopy (XPS) analysis was performed by a Kratos Axis Ultra DLD photoelectron spectrometer using monochromatic Al Ka (1486.7 eV) X-ray irradiation. High-resolution spectra were collected after loading the samples in ultra-high vacuum with an analysis area of 300µm - 700 µm and a 20 eV pass energy.

The *in-situ* Ga *K*-edge (10367 eV) X-ray absorption spectra (XAS) were collected at the CLÆSS beamline of the ALBA Synchrotron (Barcelona, Spain). The beam (200×800 µm) was collimated, and the higher harmonic were reflected with Rh-coated mirror at 3.35 mrad. The beam was monochromatized by a channel cut Si (311) double-crystal monochromator (**Figure S3, SI**). The XAS analysis of Ga/TiO_2 catalyst was conducted under three different conditions: (1) a bias was applied across the composite maintained in air without light irradiation, (2) the composite was irradiated and polarized in air, and (3) the composite was only illuminated in the presence of different

gases (He, O_2, and CH_4). For experiments (1) and (2) which involved an electric field, the prepared Ga/TiO_2 catalyst (30 mg) was packed into a quartz capillary (O.D. = 2 mm), then two electrodes were connected to each end of the catalyst pellet. Afterward, the capillary was kept under atmospheric pressure, stabilized on a metallic frame, and the opposite ends of both electrodes were plugged into a power supply. During the measurements, XAS spectra were recorded via the fluorescence mode (using a 4-channel SDD detector) while the applied bias was changed (0 – 25 V) and the light irradiation switched off or on for the experiment (1) or (2). Meanwhile, the experiments (3) were carried out under feeding gases, including He, O_2 (21% in He) and CH_4 (100%), respectively, by using only light irradiation. The results were collected and processed with Athena software.

Kelvin probe force microscopy (KPFM) was carried out with a Dimension D3100 AFM (Bruker) operating under ambient conditions in amplitude-modulation (AM)-lift KPFM mode with a Pt/Ir coated silicon probe (SCM-PIT-V2). In the first pass, the microscope operated in tapping mode, then the tip was lifted by 50 nm, and an AC + DC bias was applied to the tip. The amplitude of the AC component was set to 5 V and its frequency (56.62 kHz) close to the resonant frequency of the probe, while the KPFM feedback loop adjusted the DC bias to nullify the oscillation of the probe. As a result, its value was equal to the contact potential difference (CPD) between the tip and the sample. We first imaged the area of interest at 0 V bias, to determine a reference for the CPD. It is about +20 mV in the data relative to the 2nd KPFM experiments. On 5

locations across the device, 1 μm scans with slow scan axis disabled were performed while increasing the sample bias from 0 to +8 V by step of 2 V.

Continuous wave (CW) EPR measurements were performed at 100 K with a Bruker Elexsys E500 spectrometer operating in X-band (9.8 GHz). The samples were filled into 4 mm quartz tubes and illuminated within the cavity using LIGHTNINGCURE Spotlight source LC8. All the spectra were collected with the following conditions: 2 mW of microwave power, modulation amplitude of 1 Gauss and a conversion time of 40 ms. The formation of reactive oxygen species (ROS) upon UV irradiation was monitored via the EPR spin trapping technique at room temperature, using 5-(Diisopropoxyphosphoryl)-5-methyl-1-pyrroline-N-oxide (DIPPMPO) as spin trap agent. The spin trapping experiments were performed with [DIPPMPO]=30mM, microwave power of 10 mW, modulation amplitude of 0.2 Gauss and a conversion time of 5 ms.

2.4. Photocatalytic tests

The photocatalytic coupling methane oxidation over Ga-based catalysts and metal oxides was performed in a stainless-steel batch reactor (250 mL) equipped with a transparent window on the top irradiated with a solar simulator (Hg-Xe 400W, NEWPORT), as shown in **Figure S4, SI**. To supply electricity to the photocatalysts, two electric wires were inserted throughout the reactor lid feedthroughs, which were subsequently connected with two chip electrodes to hang up the photocatalytic chips in the middle of the reactor. For methane oxidation, the batch reactor was evacuated by a vacuum pump for 10 min, then refilled with a gas mixture of CH_4/Air (9.5/0.5 bar),

kept in dark condition within 30 min before being exposed to light irradiation. The reactor temperature was always maintained at 25 ^{o}C by a chiller during reactions. However, under light irradiation and electricity supply, the real temperature was 5° C higher, as determined by the thermocouple placed in the reactor. After the reaction, the gaseous products were directly injected and analyzed by gas chromatography (GC, Aglient 8860) combined with a flame ionization detector (FID) and a thermal conductivity detector (TCD).

3. Results and discussion

Photocatalytic oxidation of methane over Ga-supported photocatalysts

TiO_2 and ZSM-5 have been used as supports for Ga deposition. Despite the annealing of the composites at 250 °C, transmission electron microscopy (TEM) and scanning electron microscopy (SEM) combined with energy dispersive spectroscopy (EDS), performed at room temperature prior to the photocatalytic experiments, show that Ga appear as nanoparticles in both supports, as respectively visible in **Figure 1a, b**, and **S5a, b**, **SI**. These observations are consistent with the poor wettability of liquid metals on both supports because of their ultrahigh surface tension [20], which is still above 650 mN/m for Ga at 250°C [21]. The XRD patterns of catalysts reveal distinct crystalline phases of TiO_2 with additionally a broad peak of metallic Ga at $2\theta \approx 35°$ (**Figure S6, SI**). We note that the Ga nanoparticles in the supports are strongly oxidized, which was evidenced with X-ray photoelectron spectroscopy (XPS) in agreement with the literature (**Figure S7, SI**) [22–25].

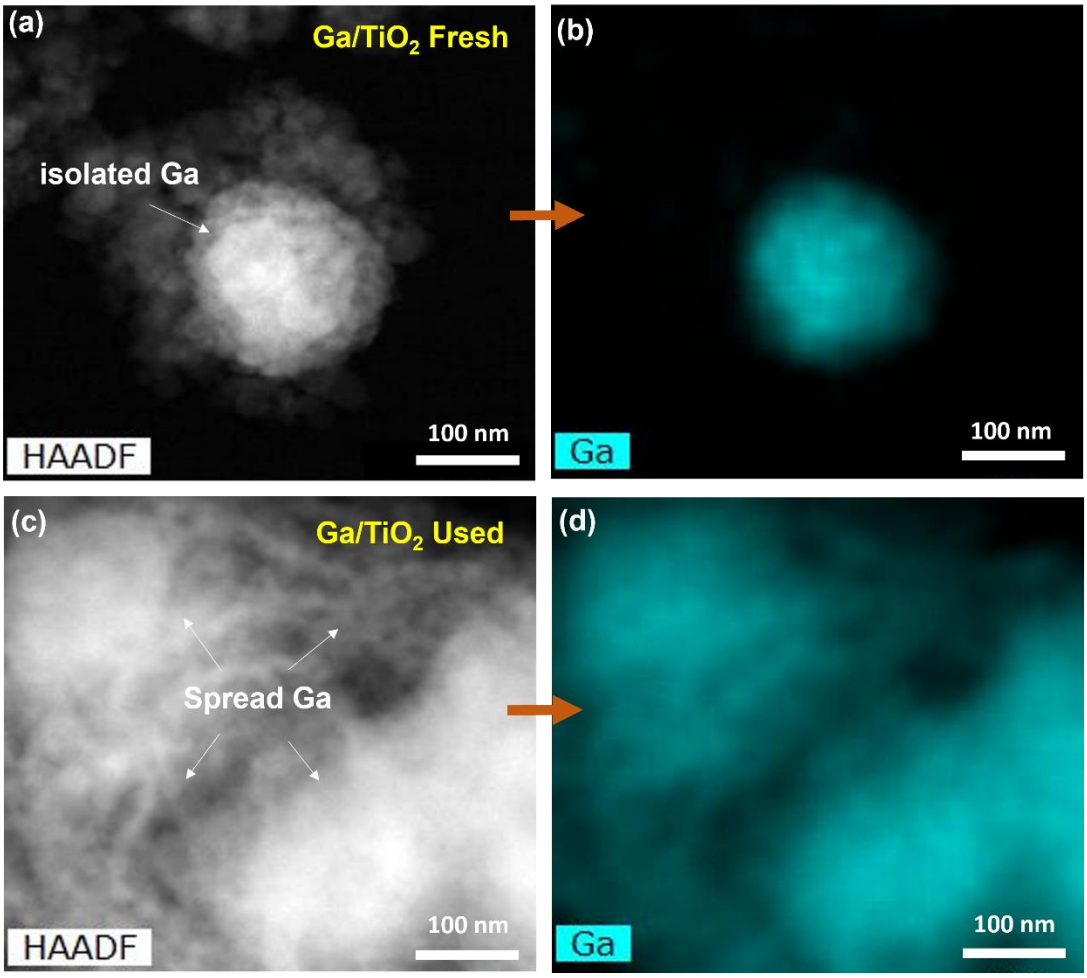

Fig. 1. *HAADF-STEM images (a, c) and the corresponding EDS mapping of (b, d) Ga for fresh and reacted Ga/TiO_2 composites, respectively. The reaction consisted of the photooxidation of methane with the chips polarized at 25 V and thermalized at 30 °C in a CH_4/Air atmosphere with a ratio of 9.5/0.5 for 6 hours.*

The structure of the composite was also characterized by cross-sectional SEM. **Figure 2a** shows a SEM image of the Ga/TiO_2 photocatalytic chip acquired at the position of the gold electrode. The average thickness of the Ga/TiO_2 photocatalyst is 15 µm. A similar photocatalyst thickness was used for all the chips prepared either with pristine TiO_2 and H-ZSM-5 powders or with Ga loaded into both photocatalysts (Ga/TiO_2, Ga/ZSM-5). Although photocatalysis mostly occurs at the surface of the

catalyst layer, such a thickness ensures that the whole area of the chip, in particular the side electrodes, is homogeneously covered by the four different photocatalysts. Control experiments for the photocatalytic oxidation of methane reactions were first performed and did not show any photocatalytic activity without light irradiation or in the absence of catalysts in the batch reactor (**Figure S8, SI**). Applying a voltage of 25 V across the chips without light could not activate the CH_4 molecules as well. Upon light irradiation, TiO_2 could generate a small amount of gases including H_2, C_2H_6, CO and CO_2 (less than 200 $\mu molg^{-1}$ in total) (**Figure 2b**), whereas H-ZSM-5 was not active (**Figure S8, SI**). Adding Ga to TiO_2 led to enhanced photocatalytic activities compared to the bare TiO_2 powder. Loading Ga into H-ZSM-5 also triggered the reaction (columns labeled "L" experiment in **Figure 2b**).

We attribute these changes of activity between the different photocatalysts to the variation of the band gap of the host powders and the presence of gallium. The band gaps of ZSM-5 and P25 TiO_2, the latter consisting of a mixed phase of rutile and anatase nanocrystals, are 4.51 eV and 3.03 eV respectively [26,27]. Therefore, they are able to absorb a limited part of the UV spectrum emitted from the Hg-Xe lamp and thereafter generate electron-hole pairs, the amount of photogenerated charge carriers increasing as the band gap gets smaller. However, oxide materials host numerous defects, in particular oxygen vacancies, which act as efficient electron-hole recombination centres. Because the recombination rates are faster than the time required to enable the reduction and oxidation of adsorbates at their surface [28], these losses combined with a small concentration of charge carriers account for the absence of products in the

photocatalysis of methane with H-ZSM-5 after 6 hours, as seen in **Figure S8, SI**. Although the losses are known to affect the activity of TiO_2, the photogeneration of a higher concentration of electron-hole pairs ensures that a fraction of the photoexcited charge carriers reaches the surface, activates the reactants and produces a small amount of H_2, C_2H_6, CO and CO_2.

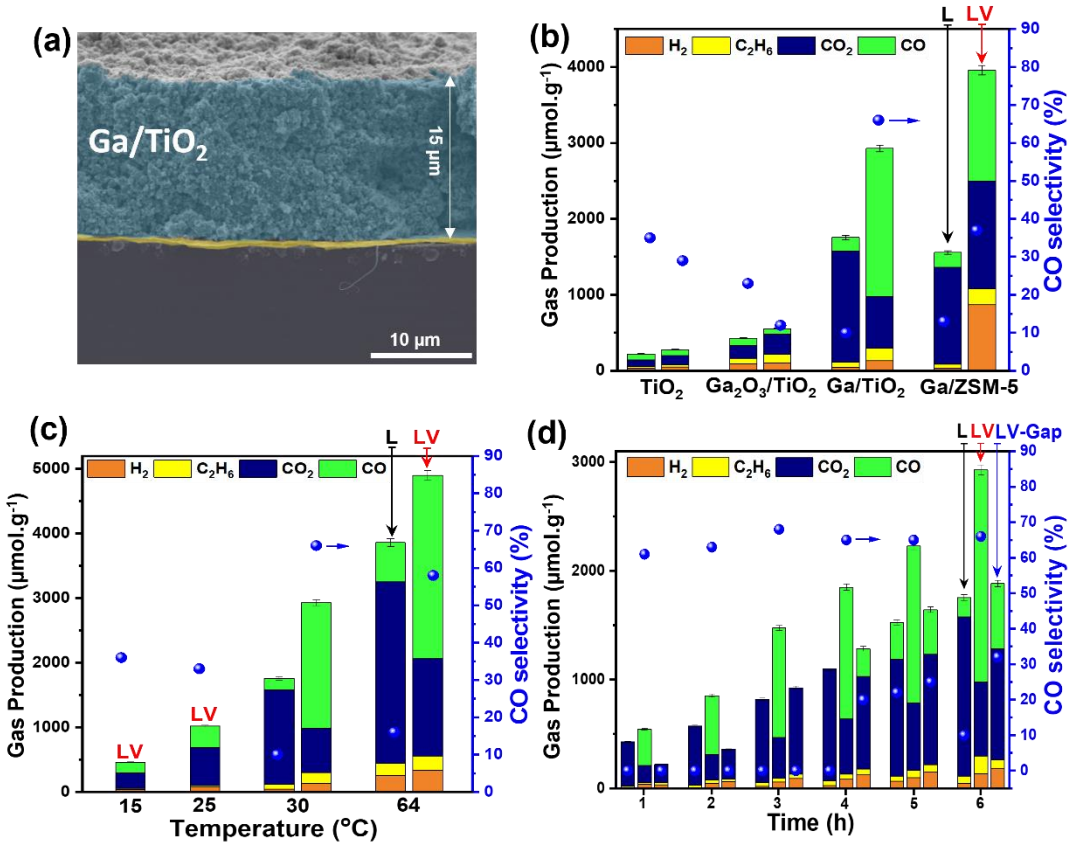

Figure 2. *(a) False color cross-sectional SEM image of Ga/TiO_2 photocatalytic chip acquired at the position of the gold electrode (from the top: the Ga/TiO_2 catalyst layer, the thin gold electrode layer, and the glass substrate). (b) Influence of a DC voltage applied across TiO_2, Ga_2O_3, Ga/TiO_2 and Ga/ZSM-5 chips on the photooxidation of methane. "L" and "LV" stand for experiments carried out under light irradiation only (Hg-Xe lamp 400W) or combined with a DC voltage of 25 V. (c) Photocatalytic methane*

oxidation efficiency of Ga/TiO_2 as a function of temperatures for an unbiased chip and a polarized chip. (d) Gas production evolution over time for the photocatalytic methane oxidation between chips fully covered with Ga/TiO_2 (labeled L and LV) or consisted of a small gap in the middle of the chip (LV-gap). Photocatalytic parameters: CH_4/Air pressure ratio of 9.5/0.5, reaction time of 6 hours in (b) and (c), reaction temperatures of 30 °C in (b) and (d). The error bars represent the standard deviation (SD) for three independent measurements.

Loading gallium into the pristine powders strongly enhanced the gas production. To get insight into the physical mechanism at the origin of such an enhancement, photoluminescence (PL) experiments were performed with the TiO_2-based photocatalytic chips (**Figure S9, SI**). Upon the optical excitation of the pristine TiO_2 chip, a green emission was observed. This sub-band gap emission involves the radiative recombination of electrons in the conduction band and in shallow levels below the conduction band with trapped holes in deep levels [29,30]. When the P25 TiO_2 powder contains gallium, the PL peak is reduced by a factor of more than three. This observation is similar to the variation of the PL emission measured when gold nanoparticles are loaded into P25 TiO_2. The quenching of the PL is the signature of a reduction of the probability for photoexcited electrons to radiatively recombine with holes in TiO_2 [12,31]. Alike gold, gallium scavenges the photoexcited electrons, giving enough time to the photoexcited holes to react with methane. The metallic nature of gallium in the composite is strongly supported by the comparison of the gas production obtained with Ga_2O_3 nanoparticles loaded in the TiO_2. While the Ga_2O_3 nanoparticles

are homogenously distributed in the TiO_2 support (**Figure S10, SI**), this chip produces a much smaller amount of gas (**Figure 2b**). We believe that the same effect occurs in ZSM-5. Despite the small concentration of photogenerated electron-hole pairs, the loading of gallium enables their efficient separation, which gives them enough time to subsequently activate the reactants.

To further assess the benefits of metal gallium loaded in the oxide materials, the chips were polarized with a bias of 25 V. Upon biasing the Ga/TiO_2 chips, the photocatalysis of methane yielded a higher total gas production. Interestingly, the ratio between the different products changed, with a significant shift between the production of CO_2 and CO. This effect was already visible after one hour of reaction and continuously increased with longer reaction times, as shown by the comparison of the columns labelled "L" and "LV" in the histogram of (**Figure 2d** and **S11a, b, SI)**. After 6 hours, the Ga/TiO_2 catalyst showed a significant improvement in the production rates and a high CO selectivity of 70% compared to 13% for conventional photocatalytic tests. This selectivity does not degrade over the number of cycles, when the samples are regenerated by applying 20 V during 10 hours in N_2 gas (**Figure S12, SI**). The same phenomenon arouses for Ga/ZSM-5, in which CO production selectivity was also enhanced upon biasing the chip (**Figure 2b** and **S11c, d, SI)**. Therefore, the polarization of the chips loaded with gallium has a strong impact on gas production and selectivity.

Wettability of the host matrix by liquid gallium

First, we dismiss an enhancement of the gas production by the electric field based on quantum confinement effects in the semiconductor host matrix. Kelvin probe force microscopy (KPFM) showed a linear drop of the potential across the Ga/TiO_2 chip

(**Figure 3a-d**), in agreement with the variation of the potential measured in Au/TiO_2 chips [12]. This smooth and continuous variation of the potential rules out the existence of intense and localized electric fields, which are usually required to ensure the separation of the photoexcited charge carriers in semiconductor nanocrystals, the so-called Stark effect [32,33]. Then, we note that the significant change of selectivity is seen above the melting temperature of gallium. At lower temperatures of 15 - 25 ^{o}C, biasing the samples during photocatalysis has much less effect (**Figure 2c**). For example, at 25°C, the percentage of CO among a total of 1000 µmol g^{-1} of gas was 33% only. As gallium is a metal with a melting temperature of 29.8 °C, it is essential to determine its distribution in the composites for a deeper understanding of the enhanced conversion of methane and the change of selectivity. Hence, the powders loaded with gallium were investigated with electron microscopy and energy-dispersive spectroscopy not only before the reaction but also after the photooxidation of methane. In contrast to **Figure 1a, b**, when the chip was operated at 30 °C, gallium does not appear localized in a nanoparticle anymore, but, instead, the Ga atoms have spread over the whole support overlapping with Ti, as shown in **Figure 1c, d** and further emphasized by additional HAADF-STEM images acquired in Ga/TiO_2 over well-separated areas (**Figures S13, SI)**. This change is also confirmed on a larger scale. For instance, when the Ga/ZSM-5 composite is studied by SEM (**Figures S5c, d, SI**), the mapping of Ga clearly shows the spreading of the Ga atoms after the reaction performed slightly above the Ga melting temperature with a bias of 25 V applied to the chip.

The strong viscosity of liquid gallium at its melting point (2.037 mPa.s vs 0.798 mPa.s for water) [34], and its high surface tension (~700 mJ/m^2), alike other liquid metals [21,35] are known to prevent liquid gallium from wetting solids. Therefore, liquid gallium keeps the shape of a nanoparticle, even at high temperatures. However, in the presence of an electric field, the surface tension of liquid metals lowers, because of its dependence on the electrostatic energy and hence on the electric potential applied between both electrodes (Lippmann equation) [36,37], improving the wettability of the liquid metal. By applying a bias to the chip, the wettability of the host matrix is strongly enhanced and favors the motion of liquid gallium into the porous host matrix [32]. To validate this hypothesis, the contact angle of a macroscopic liquid Ga droplet on Ga/TiO_2 was measured as a function of applied bias, as seen in **Figure S14**. Apparently, the droplet flattens on the host matrix with increasing bias, corresponding to contact angles more and more obtuse. This phenomenon is consistent with the one deduced from electron microscopies, indicating an enhanced wettability of liquid metal Ga under electric field. It accounts for the homogeneous distribution of gallium after the electrically-assisted photocatalytic reaction, as observed with electron microscopies. Due to the stronger penetration of liquid gallium into the TiO_2 or ZSM-5 powders, a larger portion of these matrices are in intimate contact with gallium. **Figure 2c** supports this finding. Although an increase of the temperature reduces the surface tension of liquid gallium, the wettability of TiO_2 at 64 °C and zero bias is not as high as the one induced by the electric field. When the chip is not polarized, a weaker penetration of gallium into the host matrix makes the gas production weaker. This change is explained

by the smaller fraction of the host matrix interacting with gallium, resulting in a much less effective charge separation. This phenomenon is not only visible at 64 °C, but as soon as gallium becomes liquid. The cosines of the electrowetting contact angle varies with the square of the applied voltage. Therefore, by increasing the voltage, the contact angle is reduced, improving the wetting of gallium liquid [36]. This dependence on the voltage was clearly evidenced when a bias of 50V, twice the one commonly used, gave rise to an increase of the gas production by a factor of more than 1.5 (**Figure S15, SI**).

To clarify the role played by the electric field, catalytic tests have been performed with the Ga/TiO_2 and Ga/ZSM-5 chips where a narrow gap was defined in their middle (**Figure S16, SI**). Even with such a small empty space, which prevents any electric current from flowing across the chips, the polarized chips yielded the same production as the chips entirely covered with the photocatalysts but maintained at zero bias (**Figure 2d** and **Figure S17, SI**). Again, the external electric field applied across the chips ensures an efficient penetration of liquid gallium into the host material, increasing the contact area between the semiconductor host matrix and the metallic gallium. However, at this point, the improved wettability of the host matrix thanks to the electric field does not explain the change of selectivity when the chip is polarized. In particular, the comparison of the products between both types of chips, the ones fully covered by the composites and the ones with a narrow gap, does not show the same selectivity.

Origin of the high CO selectivity

As an essential component for the methane oxidation reaction, the oxidation state of Ga element was carefully investigated by advanced XANES measurements. A full potential finite difference method of FDMNES code [38,39] was used to simulate Ga

K-edge XANES spectra of metallic Ga and three phases of Ga_2O_3, corresponding to the rhombohedral α-Ga_2O_3, monoclinic β-Ga_2O_3 and orthorhombic ε-Ga_2O_3 crystal structures [38,40]. The simulated spectra are convoluted and normalized applying the same normalization function with Athena to compare with experimental spectra (**Figure S18, SI**). A polarization of 25 V applied to the Ga/TiO_2 composite under air condition did not significantly modify the XANES spectrum of Ga in comparison with the simulated spectrum, indicating insufficient ability of electricity to oxidize Ga metals (**Figure S19a, b, SI**). Similarly, Ga metals could not be oxidized in the presence of different gases under light irradiation alone (**Figure S19c, d, SI**). By contrast, the synergetic effects of both light and polarization were able to oxidize the Ga particles, indicated by the raising line of Ga metals heading to the Ga_2O_3 region (**Figure 3e**). A qualitative comparison of the Fourier transform EXAFS spectra of the sample with reference materials (**Figure 3f**) demonstrates the presence of Ga-O bond at distances between 1− 2 Å, similar to β-Ga_2O_3. Their concentration increased with the applied voltage, but was limited, based on the comparison of the XANES spectra between Ga/TiO_2 and the Ga_2O_3/TiO_2 composite.

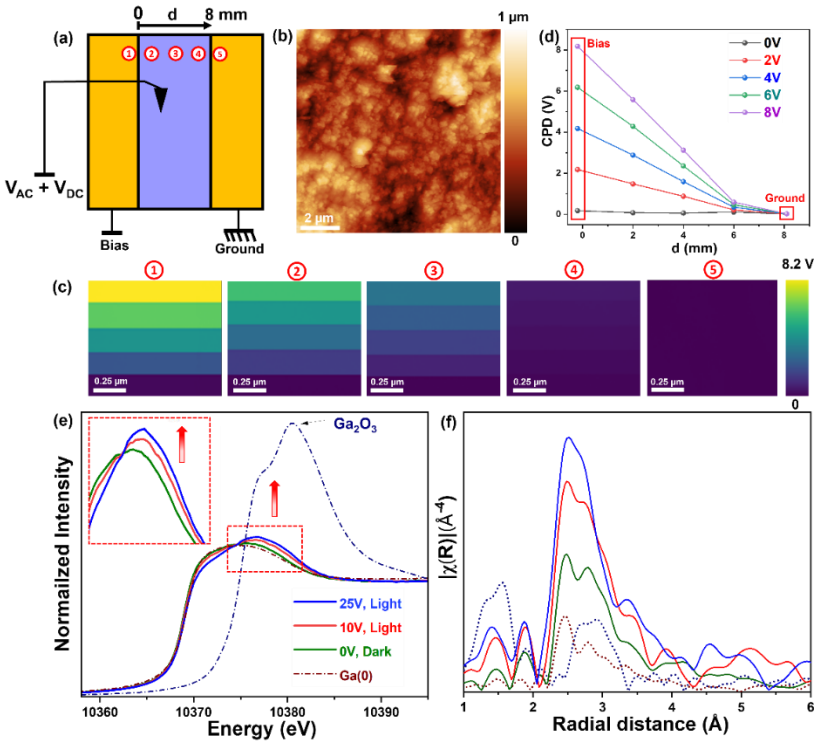

Fig. 3. *(a) Schematic illustration of KPFM measurement performed on the Ga/TiO_2 chip at five different positions. (b) AFM topography image of the Ga/TiO_2 sample surface (10×10 μm^2). (c) Contact potential difference (CPD) lines measured with increasing applied biases in the five areas defined in (a). (d) Variation of CPD as a function of the distance d under different voltages applied. (e, f) Normalized in-situ XANES and phase-uncorrected Fourier transform EXAFS spectra for Ga K-edge of Ga/TiO_2 sample under spontaneous light irradiation and different voltages (0, 10, and 25 V) for 30 minutes.*

While the oxidation process could be caused by the interaction of the spreading liquid of gallium with the TiO_2 matrix, the air used during the photocatalysis provides the major amount of oxygen at the surface of the Ga nanoparticles to oxidize gallium. Once the oxidation starts, the mechanism that drives the oxide growth relies on the formation of an internal electric potential across the interfacial oxide, called the Mott

potential [41]. We emphasize that this electric field is different from the external field applied by the power supply. It arises due to the adsorption of oxygen atoms at the metal–air interface which generates accessible surface states with an energy more positive than the filled valence band of the oxide, and more negative than the work function of the metal. As long as the interfacial oxide is thin, electrons can tunnel through the thin Ga oxide, resulting in a high density of electrons at the surface of the gallium particles wetting the TiO_2 matrix.

We believe that the formation of the thin charged oxide layer on the surface of liquid gallium is crucial to modify selectivity. To get a deeper insight into the surface reactivity of the composite, the photocatalytic oxidation of carbon monoxide by the Ga/TiO_2 chips was studied. The production of CO_2 from CO is strongly reduced when the chips were polarized with a DC voltage of 25 V (**Figure S20a, SI**), consistent with the change of selectivity observed for the photooxidation of methane when the chips were biased. As an additional experiment, a freshly-prepared Ga/TiO_2 chip was exposed to 5 bars of CO gas for 3 hours to enable the adsorption of CO molecules at the surface of the photocatalyst. Afterwards, the batch reactor was evacuated and flushed several times before filling with pure N_2 medium (5 bars). Then, the Ga/TiO_2 chip was polarized at 25 V. A CO gas signal measured with TCD evidenced the CO desorption, which readily increased for 20 hours while the chips remained polarized (**Figure S20b, SI**). It should be noted that the used Ga/TiO_2 demonstrates significantly higher CO desorption compared to the fresh catalyst, which can be attributed to the presence of an oxide layer on its surface. All these experiments agreed with the presumed existence of negative

charges at the oxide skin, which hinder the adsorption of CO molecules for the reaction. This effect is consistent with the experimental observations and theoretical predictions that a high electron density on the surface of graphene weakens the adsorption of CO [42–44]. Also, our results agree with the extremely weak adsorption of CO on GaO^+ sites found in Ga/ZSM-5 [45]. Therefore, the charging of the thin oxide layer surrounding the spread of the gallium drops is essential to repel CO molecules. The shortage of CO molecules at the surface of the photocatalyst eventually limits their subsequent reactions with O_2 species, affecting the CO_2 production.

Based on these findings, the methane conversion over the polarized Ga/TiO_2 and Ga/ZSM-5 chips is summarized in **Figure 4** and involves the following steps. First, photoexcited hole (h^+)-electron (e^-) pairs are generated in the valence (VB) and conduction (CB) bands of the host oxide crystals. Gallium loaded as co-catalyst in these matrices scavenges the photoexcited electrons, which leads to an efficient charge separation and a longer availability of the photoexcited charge carriers to take part in the chemical reaction. Hence, the photogenerated holes (h^+) migrate to the TiO_2 surface and react with the adsorbed CH_4 molecules to form methyl radicals ($CH_3^{\cdot}$) and protons (H^+). These latter combine to form H_2 and C_2H_6 products at the end [11]. Simultaneously, the photoelectrons (e^-) transferred from the CB edge of TiO_2 nanocrystals to the Ga drops oxidized the adsorbed O_2 molecules into O_2^- species, which further react with protons (H^+) and methyl radicals ($CH_3^{\cdot}$) to produce hydroxyl radicals ($OH^{\cdot}$) and hydroxymethyl radicals ($CH_3O^{\cdot}$), respectively [9,10,46].

To investigate the generation of radicals, we used electron paramagnetic resonance (EPR) analysis (**Figure S21, SI**). Upon irradiation in the presence of air, several new paramagnetic species were detected, which can be assigned to reactive oxygen species (ROS) with $g > 2.00$ and to the surface electron trapping Ti^{3+} sites with $g < 2.00$. Under simulated reaction conditions, with Ga/TiO_2 as a catalyst and 5-(Diisopropoxyphosphoryl)-5-methyl-1-pyrroline-N-oxide (DIPPMPO) as a spin trapping agent, signals representing ·OH species were instantly detected upon light irradiation (**Figure S21, SI**). Under the abundant source of hydroxyl radicals (·OH), the hydroxymethyl ($CH_3O^{\cdot}$) radicals are converted into CO molecules. Thanks to the polarization of the chips, gallium diffuses more widely in the matrices, promoting a charge separation on a larger area which increases the total gas production. In addition, a more extended surface of liquid gallium becomes oxidized, and this oxide layer charged by electrons further repels the CO molecules. It is worthy to note that, apart from photoelectrons of TiO_2 powders created under light irradiation, the reaction also received an additional electron flow, which is generated by external bias and passed throughout spreading Ga patterns, contributing similar roles as photoelectrons. The desorption experiments (**Figure S20, SI**) clearly show the role of electron flow and Ga oxide on the surface for repulsion of CO from the surface of Ga. According to the literature the desorption of CO could be induced by phonon excitations over Ga surface in the presence of electron transport [47]. This suppresses the over oxidation of CO_2 products, leading to the production of CO as the major product.

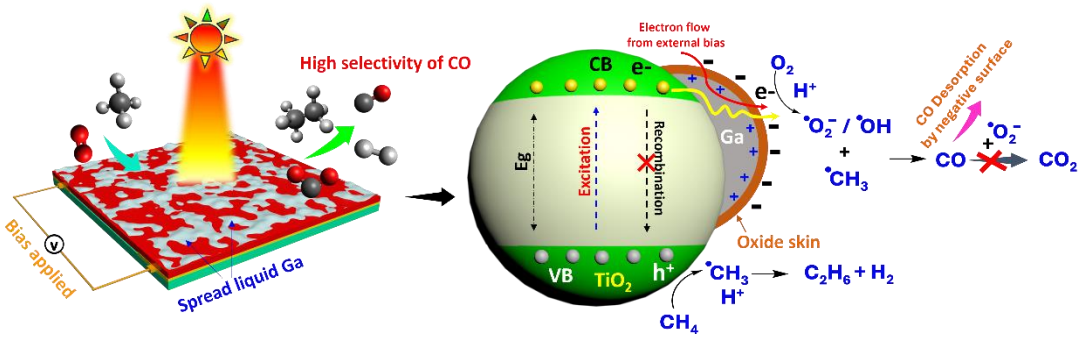

Fig. 4. *Proposed mechanism of the photocatalytic methane oxidation reaction over Ga-supported catalysts under electricity for high CO production selectivity. The band diagram shows the outcome of the photogenerated charge carriers to activate the different reactions. Under being biased, the wettability of Ga liquid metals was enhanced, which led to better penetration of Ga liquid metals on TiO_2 matrix. The oxide skin was formed when electrons in the liquid metal inner core transferred to the absorbed oxygen atoms, then the oxygen atoms get ionized reacting with Ga to form the oxide skin. The curved yellow arrow indicates photogenerated electrons passing through the inner spread liquid Ga core to oxide skin. The curved red arrow indicates an additional electron flow created by external bias applied.*

While the repulsion of CO molecules by the Ga co-catalysts requires the presence of a charged insulating surface, it is surprising that the charges can be maintained over the whole duration of the photocatalytic reaction. The absorption of oxygen on the surface of a liquid metal takes place in less than a second [41], and a surface self-limiting oxidation should be expected after a few hours. As the oxide skin around liquid gallium gets thicker, the electron cannot tunnel anymore, and the number of electrons accumulated at the surface of the oxide layer should decrease as the photocatalytic reaction proceeds. But, this is not what the XANES experiments revealed: about 1% of

Ga atoms only formed bonds with oxygen. Ga remained metallic even after 1.5 hours of light and electricity exposure. We attribute this observation to the regulation of the oxide thickness induced by electricity [48]. To account for a limited growth of the oxide layer, the electrons have to be continuously withdrawn. While a fraction of the electrons activates the reactants, the comparison of the selectivity obtained with the different chips indicates that the rest of the electrons do not accumulate, suggesting that they drift inside the polarized chips to the electrode. Although the use of semiconductor supports consisting of large band gap materials does not show a good electrical conductivity, we did measure a current of a few nanoamperes when the Ga/TiO_2 chips were illuminated (**Figure S22, SI**). Such a current is absent at zero bias or in the chips built with a gap. As a result, in a steady state, the regulation of the oxide thickness at the surface of the spread Ga drops allows the continuous transfer of electrons from the semiconductor matrix through the Ga drops to the surface of their oxidized skin. These negative charges repel the CO molecules, ensuring a high CO selectivity.

4. Conclusions

In conclusion, electricity has a profound impact on the photocatalytic oxidation of methane over liquid Ga-based catalysts. Applying a DC voltage to Ga/TiO_2 and Ga/ZSM-5 composites facilitates the spread of the liquid metal in the semiconductor supports and hence limits the severe recombination which affects oxide semiconductors. In comparison with solid metal co-catalysts, the voltage-induced wetting ability of liquid metal gives then a critical advantage to enhance charge separation and transfer. Moreover, electricity is also key to control the oxidation process at the surface of liquid

gallium, which in turn modifies the adsorption of the intermediate products and hence the selectivity of the reaction. Finally, the stability of the chips indicates the strong robustness of the liquid to catalyst poisoning. Therefore, combining electricity to liquid metal supported photocatalysts is an efficient method to accelerate photocatalytic activity and change selectivity in heterogeneous catalysis.

Acknowledgements

This project has received funding from the European Union's Horizon 2020 research and innovation programme under the Marie Skłodowska-Curie grant agreement N 847568. The authors acknowledge the support of the Chevreul institute, UCCS and IEMN PCMP−PCP platform within the RENATECH network. The XAS experiment was performed at BL22-CLÆSS beamline at ALBA Synchrotron with the collaboration of ALBA staff under experiment number 2023027488-2.

Conflict of Interest

The authors have no conflict to disclose.

Data Availability Statement

The data that support the finding of this study are available from the corresponding author upon request.

REFERENCES

[1] A.S. Loktev, V.A. Arkhipova, M.A. Bykov, A.A. Sadovnikov, A.G. Dedov, Novel Samarium Cobaltate/Silicon Carbide Composite Catalyst for Dry Reforming of Methane into Synthesis Gas, Pet. Chem. 63 (2023) 607–617.

[2] L.C.S. Kahle, T. Roussière, L. Maier, K. Herrera Delgado, G. Wasserschaff, S.A. Schunk, O. Deutschmann, Methane dry reforming at high temperature and elevated pressure: Impact of gas-phase reactions, Ind. Eng. Chem. Res. 52 (2013) 11920–11930.

[3] Y. Tang, Y. Wei, Z. Wang, S. Zhang, Y. Li, L. Nguyen, Y. Li, Y. Zhou, W. Shen, F.F. Tao, P. Hu, Synergy of single-atom Ni1 and Ru1 sites on CeO_2 for dry reforming of CH_4, J. Am. Chem. Soc. 141 (2019) 7283–7293.

[4] K. Sheng, D. Luan, H. Jiang, F. Zeng, B. Wei, F. Pang, J. Ge, NixCoy Nanocatalyst Supported by ZrO_2 Hollow Sphere for Dry Reforming of Methane: Synergetic Catalysis by Ni and Co in Alloy, ACS Appl. Mater. Interfaces. 11 (2019) 24078–24087.

[5] D. Hu, V. V Ordomsky, A.Y. Khodakov, Major routes in the photocatalytic methane conversion into chemicals and fuels under mild conditions, Appl. Catal. B Environ. 286 (2021) 119913.

[6] C. Dong, D. Hu, K. Ben Tayeb, P. Simon, A. Addad, M. Trentesaux, D.O. de Souza, S. Chernyak, D. V Peron, A. Rebai, Photocatalytic partial oxidation of methane to carbon monoxide and hydrogen over CIGS solar cell, Appl. Catal. B Environ. 325 (2023) 122340.

[7] S. Murcia-Lopez, K. Villa, T. Andreu, J.R. Morante, Partial oxidation of methane to methanol using bismuth-based photocatalysts, Acs Catal. 4 (2014) 3013–3019.

[8] X. Yu, V. De Waele, A. Löfberg, V. Ordomsky, A.Y. Khodakov, Selective photocatalytic conversion of methane into carbon monoxide over zinc-heteropolyacid-titania nanocomposites, Nat. Commun. 10 (2019) 1–10.

[9] S.V.L. Mahlaba, N. Hytoolakhan lal Mahomed, G.M. Leteba, A. Govender, E. van Steen, Role of Support in the Selective, Aerobic Methane Oxidation to Formaldehyde over Pt/TiO_2, ACS Catal. 13 (2023) 14770–14781.

[10] X. Cai, S. Fang, Y.H. Hu, Unprecedentedly high efficiency for photocatalytic conversion of methane to methanol over Au–Pd/TiO_2–what is the role of each component in the system?, J. Mater. Chem. A. 9 (2021) 10796-10802.

[11] S. Wu, X. Tan, J. Lei, H. Chen, L. Wang, J. Zhang, Ga-Doped and Pt-Loaded Porous TiO_2-SiO_2 for Photocatalytic Nonoxidative Coupling of Methane, J. Am. Chem. Soc. 141 (2019) 6592–6600.

[12] M.N. Tran, M. Moreau, A. Addad, A. Teurtrie, T. Roland, V. De Waele, C. Dong, P. Simon, K. Ben Tayeb, M. Dewitte, L. Thomas, D. Mele, V. Ordomsky, B. Grandidier, Boosting Gas-Phase TiO_2 Photocatalysis with Weak Electric Field Strengths of Volt/Centimeter, ACS Appl. Mater. Interfaces. 16, (2024) 14852–14863.

[13] J. Ran, J. Zhang, J. Yu, M. Jaroniec, S.Z. Qiao, Earth-abundant cocatalysts for semiconductor-based photocatalytic water splitting, Chem. Soc. Rev. 43 (2014)

7787–7812.

[14] X. Sun, H. Li, Recent progress of Ga-based liquid metals in catalysis, RSC Adv. 12 (2022) 24946–24957.

[15] K. Zuraiqi, A. Zavabeti, J. Clarke-Hannaford, B.J. Murdoch, K. Shah, M.J.S. Spencer, C.F. McConville, T. Daeneke, K. Chiang, Direct conversion of CO_2 to solid carbon by Ga-based liquid metals, Energy Environ. Sci. 15 (2022) 595–600.

[16] M. Armbrüster, G. Wowsnick, M. Friedrich, M. Heggen, R. Cardoso-Gil, Synthesis and catalytic properties of nanoparticulate intermetallic Ga-Pd compounds., J. Am. Chem. Soc. 133 (2011) 9112–9118.

[17] Y. Zhou, S. Santos, M. Shamzhy, M. Marinova, A.M. Blanchenet, Y.G. Kolyagin, P. Simon, M. Trentesaux, S. Sharna, O. Ersen, V.L. Zholobenko, M. Saeys, A.Y. Khodakov, V. V. Ordomsky, Liquid metals for boosting stability of zeolite catalysts in the conversion of methanol to hydrocarbons, Nat. Commun. 15 (2024) 1–10.

[18] N. Taccardi, M. Grabau, J. Debuschewitz, M. Distaso, M. Brandl, R. Hock, F. Maier, C. Papp, J. Erhard, C. Neiss, Gallium-rich Pd–Ga phases as supported liquid metal catalysts, Nat. Chem. 9 (2017) 862–867.

[19] D. Esrafilzadeh, A. Zavabeti, R. Jalili, P. Atkin, J. Choi, B.J. Carey, R. Brkljača, A.P. O'Mullane, M.D. Dickey, D.L. Officer, Room temperature CO_2 reduction to solid carbon species on liquid metals featuring atomically thin ceria interfaces, Nat. Commun. 10 (2019) 1–8.

[20] Q. Song, Y.J. Zheng, Y.J. Huang, Z.G. Xu, W.G. Sheng, J. Yang, Emergency Drug Procurement Planning Based on Big-Data Driven Morbidity Prediction, IEEE Trans. Ind. Informatics. 15 (2019) 6379–6388.

[21] S. Handschuh-Wang, F.J. Stadler, X. Zhou, Critical review on the physical properties of gallium-based liquid metals and selected pathways for their alteration, J. Phys. Chem. C. 125 (2021) 20113–20142.

[22] A.I. Serykh, M.D. Amiridis, In-situ X-ray photoelectron spectroscopy study of supported gallium oxide, Surf. Sci. 604 (2010) 1002–1005.

[23] V.I. Nefedov, Y. V Salyn, E.P. Domashevskaya, Y.A. Ugai, V.A. Terekhov, A study by XPS and XRS of the participation in chemical bonding of the 3d electrons of copper, zinc and gallium, J. Electron Spectros. Relat. Phenomena. 6 (1975) 231–238.

[24] J. Čechal, T. Matlocha, J. Polčák, M. Kolíbal, O. Tomanec, R. Kalousek, P. Dub, T. Šikola, Characterization of oxidized gallium droplets on silicon surface: An ellipsoidal droplet shape model for angle resolved X-ray photoelectron spectroscopy analysis, Thin Solid Films. 517 (2009) 1928–1934.

[25] A.I. Serykh, M.D. Amiridis, In situ X-ray photoelectron spectroscopy study of gallium-modified MFI zeolite, Surf. Sci. 603 (2009) 2037–2041.

[26] D.O. Scanlon, C.W. Dunnill, J. Buckeridge, S.A. Shevlin, A.J. Logsdail, S.M. Woodley, C.R.A. Catlow, M.J. Powell, R.G. Palgrave, I.P. Parkin, Band alignment of rutile and anatase TiO_2, Nat. Mater. 12 (2013) 798–801.

[27] Y. Sun, S. Fu, S. Sun, J. Cui, Z. Luo, Z. Lei, Y. Hou, Design of a SnO_2/Zeolite

Gas Sensor to Enhance Formaldehyde Sensing Properties: From the Strategy of the Band Gap-Tunable Zeolite, ACS Appl. Mater. Interfaces. 15 (2023) 53714–53724.

[28] J. Schneider, M. Matsuoka, M. Takeuchi, J. Zhang, Y. Horiuchi, M. Anpo, D.W. Bahnemann, Understanding TiO_2 photocatalysis: mechanisms and materials, Chem. Rev. 114 (2014) 9919–9986.

[29] S. Lettieri, M. Pavone, A. Fioravanti, L.S. Amato, P. Maddalena, Charge carrier processes and optical properties in TiO_2 and TiO_2-based heterojunction photocatalysts: A review, Materials (Basel). 14 (2021).

[30] F.J. Knorr, C.C. Mercado, J.L. McHale, Trap-state distributions and carrier transport in pure and mixed-phase TiO_2: Influence of contacting solvent and interphasial electron transfer, J. Phys. Chem. C. 112 (2008) 12786–12794.

[31] C. Gomes Silva, R. Juárez, T. Marino, R. Molinari, H. García, Influence of excitation wavelength (UV or visible light) on the photocatalytic activity of titania containing gold nanoparticles for the generation of hydrogen or oxygen from water, J. Am. Chem. Soc. 133 (2011) 595–602.

[32] F.F. Yun, Z. Yu, Y. He, L. Jiang, Z. Wang, H. Gu, X. Wang, Voltage-induced penetration effect in liquid metals at room temperature, Natl. Sci. Rev. 7 (2020) 366–372.

[33] Y.-H. Kuo, Y.K. Lee, Y. Ge, S. Ren, J.E. Roth, T.I. Kamins, D.A.B. Miller, J.S. Harris, Strong quantum-confined Stark effect in germanium quantum-well structures on silicon, Nature. 437 (2005) 1334–1336.

[34] K. Zuraiqi, A. Zavabeti, F.-M. Allioux, J. Tang, C.K. Nguyen, P. Tafazolymotie, M. Mayyas, A. V Ramarao, M. Spencer, K. Shah, C.F. McConville, K. Kalantar-Zadeh, K. Chiang, T. Daeneke, Liquid Metals in Catalysis for Energy Applications, Joule. 4 (2020) 2290–2321.

[35] T. Daeneke, K. Khoshmanesh, N. Mahmood, I.A. De Castro, D. Esrafilzadeh, S.J. Barrow, M.D. Dickey, K. Kalantar-Zadeh, Liquid metals: fundamentals and applications in chemistry, Chem. Soc. Rev. 47 (2018) 4073–4111.

[36] L.K. Koopal, Wetting of Solid Surfaces : Fundamentals and Charge effects ☆, Adv. Colloid Interface Sci. 179–182 (2012) 29–42.

[37] B. Yuan, Z.-Z. He, J. Liu, Effect of electric field on the wetting behavior of eutectic gallium–indium alloys in aqueous environment, J. Electron. Mater. 47 (2018) 2782–2790.

[38] S.A. Guda, A.A. Guda, M.A. Soldatov, K.A. Lomachenko, A.L. Bugaev, C. Lamberti, W. Gawelda, C. Bressler, G. Smolentsev, A. V. Soldatov, Y. Joly, Optimized Finite Difference Method for the Full-Potential XANES Simulations: Application to Molecular Adsorption Geometries in MOFs and Metal-Ligand Intersystem Crossing Transients, J. Chem. Theory Comput. 11 (2015) 4512–4521.

[39] Y. Joly, A.Y. Ramos, O. Bunău, Finite-difference method for the calculation of X-ray spectroscopies, (2022).

[40] O. Bunău, Y. Joly, Self-consistent aspects of x-ray absorption calculations, J. Phys. Condens. Matter. 21 (2009) 345501.

[41] H. Friedenstein, S.L. Martin, G.L. Munday, G. Dearnaley, A.M. Stoneham, D. V Morgan, W.F. Berg, J.A. Ramsey, J. Garlick, J.K. Roberts, N. Cabrera, N.F. Mott, Theory of the oxidation of metals The mechanism of the thermionic emission from oxide coated cathodes The growth and structure of semiconducting thin films B A Joyce Electrical phenomena in amorphous oxide films Latent image formation in photographic silv, Rep. Prog. Phys. 12 (1949).

[42] Z.M. Ao, S. Li, Q. Jiang, Correlation of the applied electrical field and CO adsorption/desorption behavior on Al-doped graphene, Solid State Commun. 150 (2010) 680–683.

[43] F. Schedin, A.K. Geim, S. V. Morozov, E.W. Hill, P. Blake, M.I. Katsnelson, K.S. Novoselov, Detection of individual gas molecules adsorbed on graphene, Nat. Mater. 6 (2007) 652–655.

[44] A. Omidvar, Charge-controlled switchable CO adsorption on FeN_4 cluster embedded in graphene, Surf. Sci. 668 (2018) 117–124.

[45] G.M. Zhidomirov, A.A. Shubin, M.A. Milov, V.B. Kazansky, R.A. van Santen, E.J.M. Hensen, Cluster model DFT study of CO adsorption to gallium ions in Ga/HZSM-5, J. Phys. Chem. C. 112 (2008) 3321–3326.

[46] Q. Zhou, X. Tan, X. Wang, Q. Zhang, C. Qi, H. Yang, Z. He, T. Xing, M. Wang, M. Wu, W. Wu, Selective Photocatalytic Oxidation of Methane to Methanol by Constructing a Rapid O_2 Conversion Pathway over Au-Pd/ZnO, ACS Catal. 14 (2024) 955–964.

[47] A. Tetenoire, J.I. Juaristi, M. Alducin, Disentangling the role of electrons and

phonons in the photoinduced CO desorption and CO oxidation on (O, CO)-Ru (0001), Front. Chem. 11 (2023) 1235176.

[48] D. Wang, X. Wang, W. Rao, Precise regulation of Ga-based liquid metal oxidation, Accounts Mater. Res. 2 (2021) 1093–1103.

Graphical abstract